CORNER REFLECTORS AS THE TIE BETWEEN INSAR AND GNSS MEASUREMENTS: CASE STUDY OF RESOURCE EXTRACTION IN AUSTRALIA

Matthew C. Garthwaite [(1)], Sarah Lawrie [(1)], John Dawson [(1)], Medhavy Thankappan [(1)]

[(1)] Geoscience Australia, Canberra, ACT 2601, Australia, Email:Matt.Garthwaite@ga.gov.au

ABSTRACT

The combination of continuous Global Navigation Satellite System (GNSS) measurements over a sparse network of points covering Australia with relatively low frequency but high spatial density observations from Interferometric Synthetic Aperture Radar (InSAR) is fundamental to the new geodetic reference frame being developed for Australia. Recognising the economic importance of improved positional accuracy and the potential for geodetic tools to contribute to an understanding of energy related issues, the Australian Government has funded an innovative regional geodetic network of GNSS survey marks and co-located radar corner reflectors. This new network has been installed in the Surat Basin, Queensland where regional subsidence is expected due to significant resource extraction from the subsurface. In this contribution we present initial observations of the a-priori line-of-sight height error derived from corner reflector response in TerraSAR-X, Sentinel-1A, RADARSAT-2 and ALOS-2 SAR imagery of the Surat Basin.

1. COMBINATION OF GNSS AND INSAR

Permanently deployed corner reflectors allow precise ground movements to be extracted from SAR acquisitions as persistent scatterers with stable phase characteristics at known positions [1, 2]. Since the signal to noise ratio from a resolution cell containing a corner reflector will be much greater than that from a resolution cell containing natural scatterers, the persistent scatterer signals can be used to validate the deformation signal measured spatially in SAR scenes using conventional differential InSAR time series techniques [3, 4]. The co-location of corner reflectors with GNSS survey marks will ensure SAR-derived deformation products can be tied to (and help constrain via deformation models) the local geodetic reference frame.

2. SURAT BASIN GEODETIC NETWORK

The increasing demand for energy in Australia has led to increased exploitation of unconventional coal seam gas reserves, particularly in the Surat and Galilee basins in Queensland. CSG production began in the Surat Basin in 2006 and reserves are currently being produced by several operators. Predictions of the magnitude of subsidence based on poroelastic modelling and gas production rates indicate subsidence on the order of a decimetre may be occurring [5]. Due to this expected signal of around 100 km wavelength, we have deployed a new permanent geodetic network over the northern Surat Basin in Queensland (Fig. 1) [6]. The network consists of 65 GNSS survey mark sites, with a subset of 40 sites having a co-located radar corner reflector. This subset of the geodetic network covers a region of approximately 20,000 km^2 in the vicinity of the towns of Dalby, Miles and Chinchilla. Permanent installation of the full geodetic network was completed in November 2014. Annual 7-day occupation campaign GNSS measurements on the survey marks and local ties between survey marks and corner reflectors are planned.

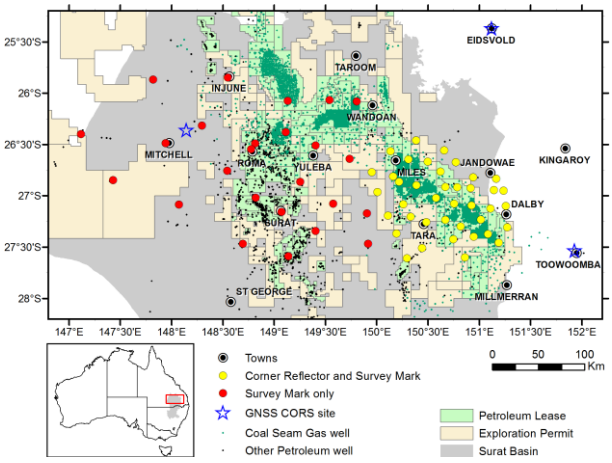

Figure 1. Distribution of 65 new geodetic sites in southern Queensland. Also plotted are land parcels designated as petroleum leases for production and exploration permits for petroleum, coal seam gas wells and other petroleum wells (as of 11 Dec 2014).

3. CORNER REFLECTOR DESIGN

We sought a single target design that would provide a bright, yet stable response in X- C- and L-band SAR imagery data and that would be stable over long (nominally decadal) time periods for permanent deployment in the landscape. A passive corner reflector was chosen over an active transponder for deployment in remote Queensland. Once deployed, corner reflectors are comparatively autonomous since transponders would require regular site visits for maintenance, continuity of power supply and transmission licencing over long time periods. Since suitable transponders [e.g. 7] are not currently commercially available, the design

and manufacture costs are also much less for a corner reflector. Furthermore, a corner reflector can more easily meet our requirement for use with different radar frequencies.

A triangular trihedral corner reflector design was chosen because of the simplicity of manufacture, long term structural rigidity, relative stability for large radar cross section and a three decibel beam width of approximately 40 degrees. This last fact ensures that the permanently deployed corner reflectors can be aligned in an average boresight orientation for all orbiting SAR sensors of interest (on either an ascending or descending orbital pass) yet the signal to noise ratio of the radar response for each SAR sensor will still be high and stable.

Since radar response is target size and radar frequency dependent we recognised that a single design would require a compromise for some radar frequency bands. We undertook a prototyping exercise to establish the most appropriate size of triangular trihedral corner reflector [8]. We manufactured 18 prototypes ranging in size from 1.0 m to 2.5 m inner leg dimension. The radar cross section (RCS) at a range of viewing angles was characterised at a ground radar reflection range. Following this characterisation, the prototypes were deployed in a temporary network near to Canberra in early 2014. During this deployment the radar response of the prototypes was tested with X- and C-band imagery from TerraSAR-X, COSMO-SkyMed, RADARSAT-2 and RISAT-1. Unfortunately the temporary deployment pre-dated the launch of the new L-band SAR satellite, ALOS-2. Results from these tests led to a corner reflector of 1.5 m inner leg length being chosen for the permanent Surat Basin geodetic network (Fig. 2) [8]. The three 2.0 m and three 2.5 m prototype corner reflectors were permanently re-deployed in the Surat Basin geodetic network.

A secondary aim of the permanently deployed corner reflectors is that they provide the international space community with a reliable means to perform ongoing radiometric, geometric, and impulse response measurements for calibration of SAR sensors on spaceborne or airborne platforms [9]. To date they have been used by ISRO, e-GEOS, JAXA and ESA to calibrate and/or validate RISAT-1, COSMO-SkyMed, ALOS-2 and Sentinel-1A SAR data.

In the Surat Basin geodetic network, most corner reflectors are installed on the soil profile of the sedimentary basin; one of the forty corner reflectors was coupled to bedrock at the ground surface. The foundation for each corner reflector, depicted in Fig. 2, comprises a suspended two metre square slab supported by four concrete pillars each of 3.0 metre length. This foundation was designed to mitigate the impact of signals originating from seasonal swelling in the upper soil layers.

Upon installation, all forty corner reflectors were aligned for ascending passes of orbiting SAR satellites. The boresight azimuth and elevation angles for ALOS-2, RADARSAT-2 and Sentinel-1A were calculated for each position, and an average of these orientations was used when aligning each corner reflector. Corner reflector positions and current alignments are given in [6].

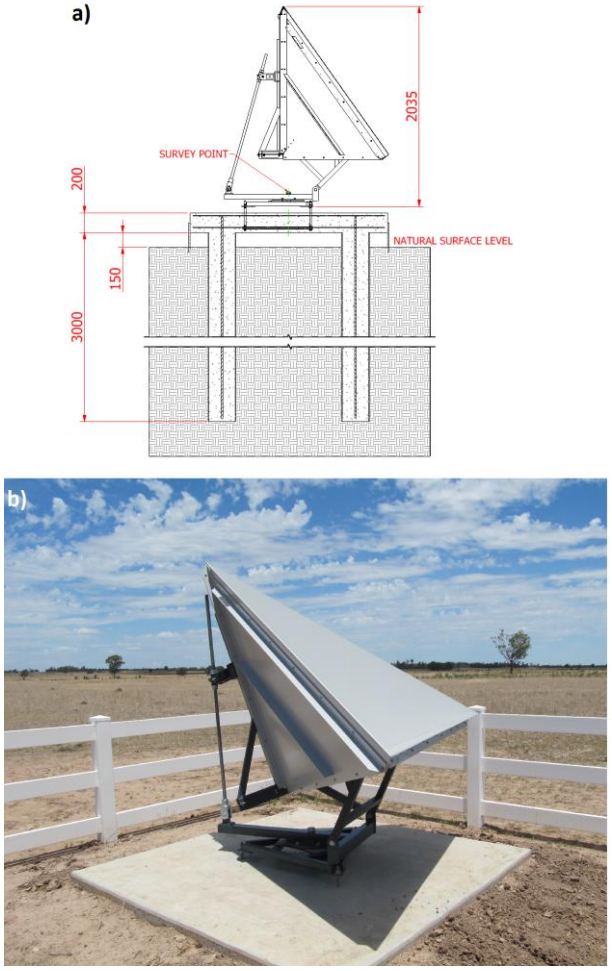

Figure 2: a) Engineering drawing of the 1.5 m triangular trihedral corner reflector (side-on view) and concrete foundation design. Dimensions in mm. b) 1.5 m corner reflector installed at Site 26. Concrete slab dimension is 2.0 m square. Most sites have a plastic fence to protect the corner reflector from livestock damage.

4. CORNER REFLECTOR RESPONSE

Corner reflector response from the Surat Basin geodetic network has been measured in data from TerraSAR-X Stripmap, RADARSAT-2 Wide-Fine, Sentinel-1A IWS mode (GRD format) and ALOS-2 Fine beam SAR imagery (Fig. 3).

To be of use as a stable phase target for temporal InSAR

analyses the corner reflector must be visible in the SAR image above the background signal level (the 'clutter'). The typically used measure of target visibility in a SAR image is the Signal-to-Clutter Ratio (SCR) [10]:

$$SCR = \frac{\sigma_T}{\langle \sigma_C \rangle} = \frac{\sigma_T}{\langle \sigma^0 \rangle A} \quad (1)$$

where σ_T is the point target RCS, $\langle \sigma_C \rangle$ is the ensemble average of clutter RCS in the vicinity of the point target.

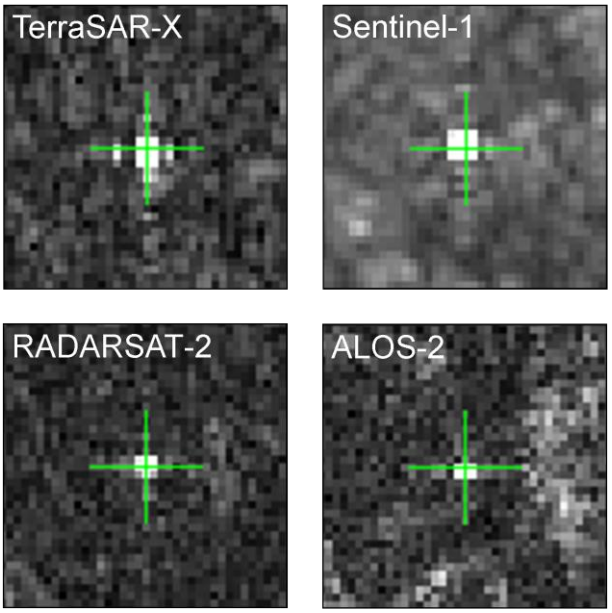

Figure 3. Impulse response for the 1.5 m corner reflector at site 6 in intensity images from each SAR sensor.

We calculate the SCR for each corner reflector in each SAR image using the method of [11] but calculating the average clutter from four windows surrounding the impulse response rather than a window with perceived low backscatter (Fig. 4). Irrespective of frequency band, we find that the corner reflectors all exceed an SCR of 20 decibels (Tab. 1). The SCR at X-band is at least 10 decibels greater than at C- or L-band.

Table 1. Statistics on SCR measurements for Surat Basin corner reflectors.

	# SAR images	# targets imaged	Mean SCR	Std. Dev.
TerraSAR-X	11	11	49.57	3.19
Sentinel-1A	3	38	32.00	2.85
RADARSAT-2	8	40	36.18	2.17
ALOS-2	11	36	29.86	6.14

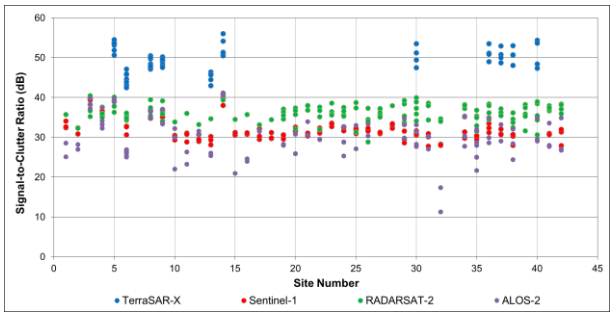

Figure 4. SCR for Surat Basin corner reflectors in X-, C- and L-band SAR imagery.

Assuming that the radar response from a single resolution cell (pixel) contains un-correlated signal from all the distributed background scatterers that fall within that cell, the probability density function for the phase error φ_{err} of a point scatterer due to the influence of distributed clutter is [12]:

$$pdf(\varphi) = \frac{\sqrt{SCR} \cdot |\cos(\varphi)|}{\sqrt{\pi}} \cdot exp^{-SCR \cdot sin^2(\varphi)} \quad (2)$$

This function implies that the phase error magnitude is determined by the point target SCR. The estimated effective phase error in radians drawn from the probability density function is [12]:

$$\varphi_{err} = \frac{1}{\sqrt{2 \cdot SCR}} \quad (3)$$

Therefore the expected phase error can be estimated a-priori using the measured point target SCR from each SAR intensity image independently [12, 13]. An alternative method for estimating the phase error a-priori is the amplitude dispersion method first described by [1]. Through a simulation exercise, [12] find that the SCR is a more effective estimator of phase error than the amplitude dispersion for SCR greater than 9 decibels. Below this threshold, an optimistic bias occurs in both methods, with the amplitude dispersion being more optimistic. Reference [13] find that both these methods are only applicable for targets with an SCR greater than 9 decibels, as is the case for all the Surat Basin corner reflectors, since phase residuals are only approximately normally distributed when the phase error magnitude is less than 0.25 radians.

The a-priori phase error can be converted to a height error in the SAR sensor line-of-sight (LOS; i.e. a slant-distance error) using the radar wavelength λ:

$$h_{err} = \frac{\varphi_{err} \cdot \lambda}{4\pi} \quad (4)$$

We refer to this as a 'LOS height error' since for most cases the vertical component has more influence on the LOS vector than the horizontal component. This is the case whenever the SAR incidence angle is less than 45 degrees.

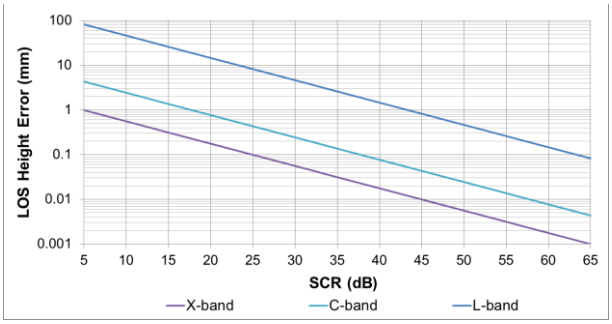

Figure 5. LOS height error h_{err} as a function of SCR for the radar frequencies of interest.

From the measured SCR values and the relationship plotted in Fig. 5 we can estimate a-priori values of LOS height error. At X-band the height error is less than a tenth of a millimetre. At C-band the height error is around a quarter of a millimetre. At L-band there is more variability in the SCR and the height error can be up to 10 mm. These LOS height errors are independent of other error sources present in interferograms such as orbital errors or atmospheric path delays. The total error in an interferogram will equal the sum of all these independent components.

5. DISCUSSION

Using the SCR as a proxy for phase error, and therefore LOS height error, should be treated with caution. Reference [13] conducted a validation experiment with five corner reflectors, comparing heights derived from ERS and ENVISAT InSAR analyses with repeated levelling surveys. From this experiment they found that the a-priori phase error derived from SCR is under-estimated by 3-4 times compared to the a-posteriori estimates. A-posteriori validation of the LOS height errors for Surat Basin corner reflectors is the subject of future work. In the meantime, a-priori LOS height error is considered a suitable quantity with which to assess the suitability of the new radar corner reflector network to detect surface movements using InSAR at different radar frequencies.

6. ACKNOWLEDGEMENTS

The geodetic network was funded by the AuScope Australian Geophysical Observing System (AGOS) project through funding from the Education Investment Fund (EIF) Round 3. TerraSAR-X and RADARSAT-2 data was purchased using AGOS funds. ALOS-2 data was provided by JAXA under CVST project 22. Sentinel-1 GRD format data was provided by ESA through the Scientific Data Hub. This paper is published with the permission of the CEO, Geoscience Australia.

7. REFERENCES

1. Ferretti, A., Prati, C., and Rocca, F. (2001). Permanent scatterers in SAR interferometry. *IEEE Transactions on Geoscience and Remote Sensing*. **39**(1), 8-20.
2. Hooper, A., et al., (2004). A new method for measuring deformation on volcanoes and other natural terrains using InSAR persistent scatterers. *Geophysical Research Letters*. **31**(23), L23611.
3. Berardino, P., et al., (2002). A new algorithm for surface deformation monitoring based on small baseline differential SAR interferograms. *IEEE Transactions on Geoscience and Remote Sensing*. **40**(11), 2375-2383.
4. Wang, H., et al., (2012). InSAR reveals coastal subsidence in the Pearl River Delta, China. *Geophysical Journal International*. **191**(3), 1119-1128.
5. Brown, N.J., et al., (2014). Constraining Surface Deformation Predictions Resulting from Coal Seam Gas Extraction. Record 2014/44, Geoscience Australia, Canberra.
6. Garthwaite, M.C., et al., (2015). A regional geodetic network to monitor ground surface response to resource extraction in the northern Surat Basin, Queensland. *Australian Journal of Earth Science*. submitted.
7. Mahapatra, P.S., et al., (2014). On the Use of Transponders as Coherent Radar Targets for SAR Interferometry. *IEEE Transactions on Geoscience and Remote Sensing*. **52**(3), 1869-1878.
8. Garthwaite, M.C., et al., (2015). Design of Radar Corner Reflectors for the Australian Geophysical Observing System, Record 2015/03, Geoscience Australia, Canberra.
9. Thankappan, M., et al. (2013). Characterisation of Corner Reflectors for the Australian Geophysical Observing System to Support SAR Calibration. In Proc. ESA Living Planet Symposium. Edinburgh, UK.
10. Freeman, A., (1992). SAR calibration: an overview. *IEEE Transactions on Geoscience and Remote Sensing*. **30**(6), 1107-1121.
11. Gray, A.L., et al., (1990). Synthetic Aperture Radar Calibration Using Reference Reflectors. *IEEE Transactions on Geoscience and Remote Sensing*. **28**(3), 374-283.

12. Adam, N., Kampes, B., and Eineder, M., (2004). Development of a scientific permanent scatterer system: Modifications for mixed ERS/ENVISAT time series. in Proc. Envisat and ERS Symposium. Salzburg, Austria.
13. Ketelaar, V.B.H., Marinkovic, P., and Hanssen, R. F., (2004). Validation of Point Scatterer Phase Statistics in Multi-pass InSAR. in Proc. Envisat and ERS Symposium. Salzburg, Austria.